SiC Device Development for High Temperature Sensor Applications

J.S. Shor, D. Goldstein, A.D. Kurtz and R.M. Osgood[*]

Kulite Semiconductor Products, Inc, Leonia, NJ

[*]Columbia University
Microelectronics Sciences Laboratories, NY, NY

Introduction

The two most common measurements of operating parameters in wind tunnels, materials processing, biomedical applications, and aeronautical propulsion systems involve temperature and pressure. As these applications become more advanced, increasing need is developing to measure these parameters in hostile environments, such as high temperatures. For example, in the wake of the current drive to reduce energy costs, commercial airlines are attempting to develop more fuel efficient engines while maintaining or even upgrading the safety factor. This need requires computer control of injection valves, fuel/air ratios and operating parameters within the engines. Therefore, it is essential to monitor pressures in different segments of the engines during flight. Since engine efficiency in turbojet engines is also greater at higher temperatures of the combustion gas, the emphasis has been to increase the operating temperatures of the engines, which can reach temperatures as high as 2000°F in sections of the engines. Thus, highly reliable, durable high temperature sensors are required. Furthermore, in order to develop such engines, test sensors are required to verify existing design codes. This category of sensor must be very precise, but need not last as long as an instrumentation sensor. Wind tunnel testing and instrumentation have similar demands on the measurement of operating parameters such as pressure and temperature. Finally, the materials processing industry also has sensor needs as diverse as the measurement of operating parameters in oil refineries, pipes, heat exchangers, etc. Very often these measurements require sensors that must be durable over a long period of time, while others, such as CVD growth, will only require cheap sensors for a one time use.

Piezoresistive sensors fill many of the requirements of these applications. The wheatstone bridge design allows the simultaneous measurement of both temperature and pressure with a high degree of accuracy. Furthermore, the development of a high temperature piezoresistive transducer involves the fabrication of strain sensing elements on a diaphragm or beam. These strain gauges can also be used for applications where a highly accurate measurement of strain at high temperatures is needed. For example, the outer skins of commercial airliners can reach temperatures as high as 1400°F. In order to design such aircraft, it is important to know the relationship of stress/strain on the frame at these temperatures.

Although silicon transducers have been reported with stable

pressure outputs at high temperatures (see Kurtz et al. in these proceedings), there are fundamental problems with using silicon as a mechanical material at temperatures above 600°C. Namely, silicon begins to undergo plastic deformation under minimal loads at these temperatures, rendering it useless as a sensing element. Furthermore, silicon becomes intrinsic at these temperatures. Thus, in order to make a sensor which will be useful at temperatures of 600°C and higher, a more temperature resistant semiconductor must be used. These problems have motivated our research into SiC.

Comparison of High Temperature Semiconductors

Table 1 lists a number of wide band gap semiconductors that are currently being researched, including Si, 3C-SiC, 6H-SiC, Diamond, GaN and GaP. In order for a material to be developed for device applications, it is necessary that the properties of the material be appropriate for the device in question and that the processing

Table I Comparison of Semiconductors

Property	Si	GaAs	GaP	β-SiC (6H SiC)	Diamond
Bandgap (eV) at 300 K	1.1	1.4	2.3	2.2 (2.9)	5.5
Maximum operating temperature (°C)	300	460	925	873 (1240)	1100(?)
Melting point (°C)	1420	1238	1470	Sublimes > 1800	Phase change
Physical stability	Good	Fair	Fair	Excellent	Very good
Electron mobility R.T., $cm^2/V-s$	1400	8500	350	1000 (600)	2200
Hole mobility R.T., $cm^2/V-s$	600	400	100	40	1600
Breakdown voltage E_b . 10^6 V/cm	.3	.4	—	4	10
Thermal conductivity σ_T , W/cm-°C	1.5	.5	.8	5	20
Sat. elec. drift vel. v(sat), 10^7 cm/s	1	2	—	2.5	2.7
Dielectric const., K	11.8	12.8	11.1	9.7	5.5
Relative Z_J	1	7	—	1100	8100
Relative Z_K	1	.5	—	6	32

$$Z_J \propto E_b^2 \, v^2(sat) \qquad Z_K \propto \sigma_T [v(sat)/K]^{1/2}$$

Table 1: Comparison of high temperature semiconductors (courtesy of J.A. Powell, NASA Lewis)

256

technology be advanced enough to allow device fabrication. Diamond can only be deposited in a polycrystalline form on non-diamond substrates, and bulk single crystal growth has not been achieved yet; thus diamond technology is too immature at this stage to be practical. GaP has poor physical stability at high temperatures and a melting point which is similar to silicon, which suggests that its mechanical properties will be inappropriate for high temperature sensors. GaN cannot be used for devices at the present time, since p-type conduction and ohmic or rectifying contacts have not been produced in GaN as of yet. However, SiC has excellent electrical and mechanical properties at high temperatures. Its wide band gap will allow p-n junctions to function at temperatures as high as 600°C. SiC has a high thermal conductivity, melting point and thermal stability at temperatures of interest. Furthermore, there is very little deterioration in the mechanical properties of SiC, such as its tensile strength up to 1800°C [1]. Of the high temperature semiconductors mentioned, SiC has the most advanced device technology associated with it*. For these reasons, it appears that SiC has the best potential for high temperature sensors. In this paper, we will review recent progress made at Kulite in the characterization and processing of 3C-SiC for sensor applications.

Piezoresistance of 3C-SiC

The piezoresistive properties of SiC have not yet been fully characterized in the literature. There was some early Russian work done on the piezoresistance of α-SiC, which has a large piezoresistive effect (e.g. high resistivity n-type 6H-SiC has $\pi_{11}=-142\times10^{-12}$ cm^2/dyne at 273°K [2]). However, there was only one study done on the piezoresistive properties of 3C or ß-SiC [3] which reported only the hydrostatic pressure coefficient $\pi_{11}+2\pi_{12}$, but did not examine the two coefficients π_{11} and π_{12} separately.

Epitaxial layers of ß-SiC were grown by CVD on silicon substrates at the NASA Lewis Research Center by previously described means [4]. These films were of the (100) orientation and were 10 μm thick. The samples were n-type with resistivities ranging between 0.1-1.0 Ω-cm and carrier concentrations $\approx 10^{16}-10^{17}$ cm^{-3}. The samples were metallized and patterned into narrow rectangular bars with metal contacts at each end. The silicon substrates were then selectively etched leaving thin SiC strips which would be used as strain gauges. Since piezoresistance is a tensor property, several gauge configurations were tested (Fig. 1). By applying a known stress along the axis of the gauges and measuring the change in resistivity, the three piezoresistive coefficients can be calculated. In our experiments, it was more convenient to apply a strain rather than a stress. Hence, the quantity measured was the gauge factor (GF), which is defined as

$\delta R/\varepsilon R$ where R=resistance and ε=strain.

A positive gauge factor corresponds to an increase in resistance

with tensile strain, while a negative GF signifies a decrease. The gauge factor is related to the piezoresistive coefficients by Young's modulus and dimensional corrections, which are small in this case. The SiC gauges were mounted onto a cantilever beam, and the beam was bent to produce a uniaxial strain. Resistivity changes were measured with applied strain. P-type Si strain gauges of known gauge factor were used as controls in order to determine the experimental error, which is estimated to be within 10%.
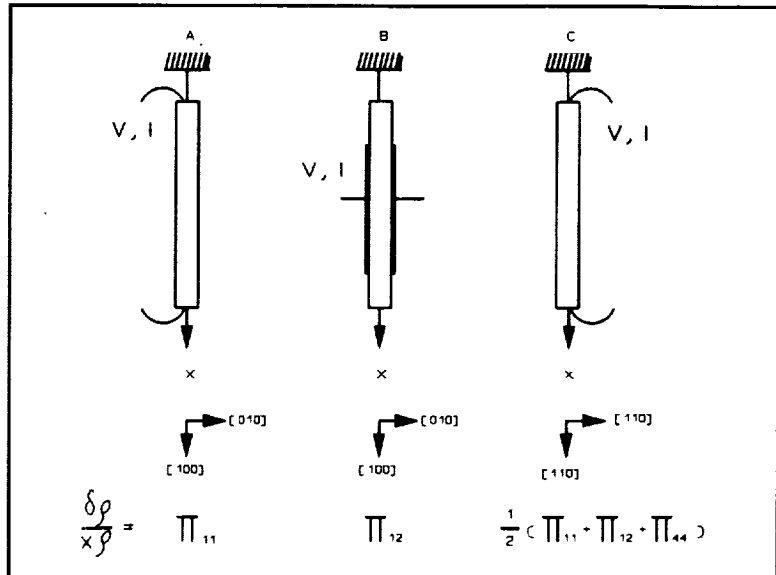

Figure 1: Three configurations used for the measurement of the piezoresistive properties of SiC.

The room temperature gauge factors for ß-SiC are listed in Table 2 along with the GF's of n-Si calculated from the literature. Configuration "A" has the largest magnitude, indicating that π_{11} is the largest of the piezoresistive coefficients for both n-SiC and n-Si. There is a small nonlinearity with strain shown by the SiC gauge factors. This effect amounts to 0.4%/100 ppm in configuration "A" with the magnitude of the GF's decreasing with tension and increasing under compression.

There are several theories found in the literature for the mechanism of the piezoresistive effect in semiconductors. In n-type material, the one that applies most often is the electron transfer effect [5]. This theory relates the change in resistivity to a redistribution of electrons among the multivalleys in momentum space. Fig. 2 is a diagram of four of the six multivalleys found in a cubic crystal. In this figure, the multivalley minima are all along a major crystallographic axis, <100>. The electron mobility is highly anisotropic within the valleys, but the symmetry of the six valleys causes the net mobility to be uniform. The application of a tensile strain in the <100> direction will cause the multivalley minima along the x-direction to rise in energy, while those in the y- and z-directions will drop. This is depicted by the dotted lines. The energy difference will cause a redistribution of the electrons between the potential wells. In a resistivity measurement along the <100> direction, more electrons will have mobilities equal to μ_t than μ_l, hence the piezoresistive effect.

258

For a lightly doped sample, Boltzman statistics can be used to estimate the value of the change in resistivity for strains applied in different configurations (e.g. Fig. 1). This analysis has been done [5], and the results indicate that for a cubic semiconductor with its multivalley minima in the <100> direction, π_{11} will be the largest coefficient with $\pi_{12} \approx -\frac{1}{2}\pi_{11}$ and $\pi_{44}=0$. It is easy to visualize why π_{44}, the shearing coefficient plays no role. A shearing strain is equal to a tension in the <111> direction and an equal and opposite compression at 90°, in the <11$\underline{1}$> direction. This will cause all of the six multivalleys to deform in the same manner, preserving the crystal symmetry.

Table 2: Room temperature gauge factors of ß-SiC

Material	resistivity (ohm-cm)	GF_A	GF_B	GF_C
n ß-SiC	0.7	-31.8	+19.2	-3.7
n Si	11.0	-133.0	+68.3	-52.0
corresponding piezoresistive coefficients		π_{11}	π_{12}	$\frac{1}{2}(\pi_{11}+\pi_{12}+\pi_{44})$

The electron transfer mechanism has been accepted as the primary effect for n-Si, which has its multivalleys in the <100> direction and piezoresistive coefficients in accord with the theory. Electron cyclotron resonance experiments on ß-SiC [6] have shown that it also has its mutivalleys in the <100> direction and a large mobility anisotropy exists within the valleys. The data in Table 2 shows that the piezoresistive coefficients of ß-SiC follow the theory closely with $\pi_{12} \approx -0.6\pi_{11}$ and $\pi_{44} < \pi_{11},\pi_{12}$. Thus, it is reasonable to assume that the electron transfer effect is the dominant mechanism for n-type ß-SiC, with smaller secondary effects playing a role as well. A more detailed description of the temperature coefficient of gauge factor and the temperature coefficient of resistivity is being published elsewhere.[†]

The electron transfer mechanism for the piezoresistive effect in semiconductors predicts a 1/kT dependence of the piezoresistive coefficients with temperature [5]. This temperature dependence is most valid at low temperatures and low doping levels. For highly doped semiconductors, both the magnitude of the piezoresistance and its dependency on temperatureare reduced. In the case of extreme degeneracy, as is seen in metals, the piezoresistive effect becomes smaller than resistance changes due to deviations in dimensionality of the gauges. However, degenerately doped semiconductors have

---

[†]J. S. Shor, D. Goldstein, and A. D. Kurtz, unpublished data.

large gauge factors compared to metals while being significantly more temperature independent than lower doped semiconductors. Therefore, degenerately doped semiconductors are generally more useful as strain sensing elements than low doped materials, since it is easier to achieve a temperature independent output with highly doped gauges.

The temperature variation of gauge factor is shown in Fig. 3, which plots gauge factor for undoped (0.2-0.7 Ω-cm, $10^{16}-10^{17}$ cm^{-3}) and degenerately nitrogen doped (0.02 Ω-cm, 10^{18}cm^{-3}) β-SiC of configuration "A". Initially, the gauge factor shows a large decrease with temperature, but levels off at 400°C. This result is similar to the behavior of lightly doped silicon strain gauges which exhibit a large temperature
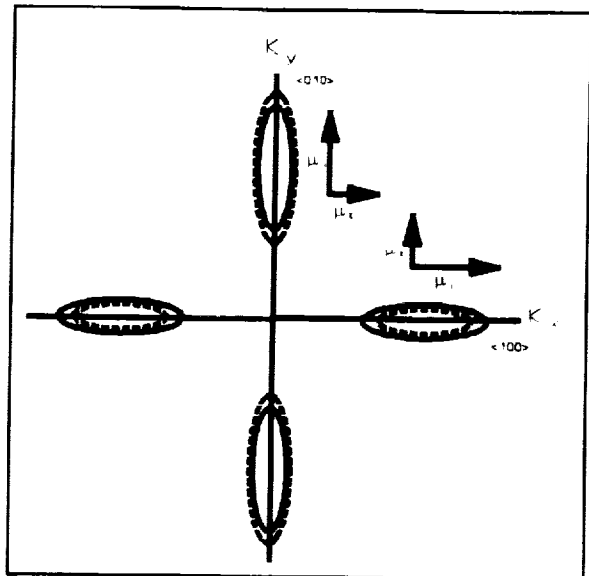

Figure 2: Energy surfaces in momentum space. Under zero strain the multivalleys are symmetric (solid lines), while this symmetry is removed under tensile strain in the <100> direction (dashed lines).

dependence at low temperatures and a reduced temperature dependence at higher temperatures [5]. The gauge factor is much more temperature independent in the case of the degenerate doping level, 10^{20} cm^{-3}. In fact, most of the temperature variation in the degenerate gauges is due to an increase in the low temperature GF's due to compression caused by mounting. It should be noted that the degenerately doped gauges of Fig. 3 had a very low gauge resistance, and a relatively high contact resistance. Measurements of gauges with Kelvin contacts indicate that the values of the GF's of the degenerately doped gauges of Fig. 3 are reduced by $\approx$ 25-40% due to the contact resistance.

All of the doping levels in n-type SiC exhibit a more temperature independent gauge factor at temperatures above 200°C. At temperatures approaching 500°C, the gauge factor appears to be almost constant with temperature. This behavior indicates that at even higher temperatures the gauge factor will retain this constant value. The gauge factor of silicon at high temperatures is between 40-60 depending on the doping level, while those of metallic gauges are between 1-2. Since the magnitude of the SiC GF at high temperatures equals 10-15, it appears that n-type β-SiC has a sufficiently high sensitivity to be useful at temperatures where silicon cannot be used.

TCR (Temperature Coefficient of Resistivity) of n-type β-SiC

In order to evaluate a piezoresistive sensing material that will be used over a wide temperature range, it is important to

understand the variation of resistivity with temperature. In Figure 4, the resistance of undoped, lightly doped and degenerately doped gauges is plotted as a function of temperature for the calculation of the TCR, which is defined as

$$TCR=\{R(T)-R(T_{ref})\}/R(T_{ref})\{T-T_{ref}\}.$$

The TCR reflects both the magnitude and direction of the dependence of resistivity on temperature. In Fig. 4, the resistivity of all three doping levels is plotted against temperature on a semi-logarithmic scale for comparison. Both the undoped and lightly nitrogen doped samples have a negative TCR at low temperatures, representing a decrease in resistance with temperature. At higher temperatures the TCR becomes positive and the resistance increases with temperature. The undoped samples exhibit a

Figure 3: Gauge factor vs. temperature for n-type ß-SiC gauges of the "A" configuration (Fig. 1).

positive TCR above -50°C,and above room temperature the TCR has an approximately constant value of 0.72%/°C. These characteristics are very similar to those exhibited by silicon samples of similar resistivity. The nitrogen doped samples are less temperature dependent than the undoped ones and have a positive TCR only above 200°C, at which point the resistance increases in a nonlinear manner. The lowest TCR is exhibited by the degenerately doped gauges, which have a positive TCR of .04%/°C at all temperatures measured.

In general, at low temperatures (typically < 0°C), the resistivity of extrinsic semiconductors will decrease with increasing temperatures due to the ionization of impurities. In this regime, the dominant scattering mechanism, impurity scattering, bears a smaller effect on the resistivity than the carrier generation does. Once the impurities are fully ionized, usually at $\approx$ 0°C, the resistivity increases due to lattice scattering, which is a larger effect than the thermal electron-hole generation. At very high temperatures, the impurity carriers are swamped by intrinsic carriers, causing the resistivity to decrease once again. This type of behavior is exhibited by ß-SiC. However, the undoped samples appear fully ionized at a much lower temperature than the lightly nitrogen doped samples (10^{18}). This effect may be
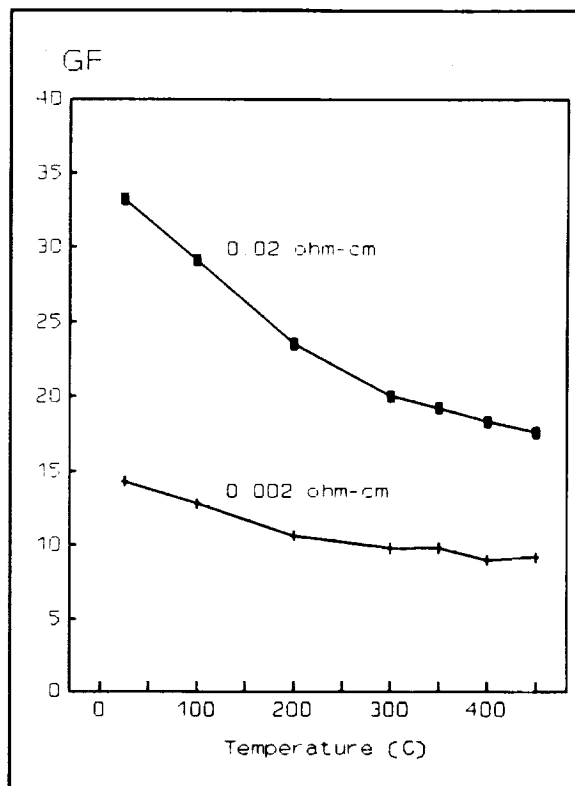
explained by the donor mechanisms that control the electrical properties of ß-SiC grown on silicon. Photoluminescence measurements [7] have determined that in the nitrogen-doped films, nitrogen is a substitutional donor with an activation energy of 40-54 meV, depending on the doping level. However, in the undoped films the principal donor, which has an activation energy of 18 meV, is not substitutional nitrogen [7]. At this time, the cause of this shallow donor is unknown. Nevertheless, it is possible, that the 18 meV donor, because of its lower activation energy, causes a lower ionization temperature in the undoped samples.

In the case of degenerately doped SiC (10^{20}cm^{-3}), the Fermi level is in the conduction band. Thus, the carriers are fully ionized at all temperatures and the TCR increases due to scattering effects.

Figure 4: TCR of n-type ß-SiC for several doping levels.

Intrinsic carrier generation was not observed in the TCR of SiC up to 800°C, because of the material's wide bandgap. As with silicon, the TCR of SiC decreases as the carrier concentration is increased. This is due to the effects of statistical degeneracy, which make semiconductors behave more like metals, which generally have very low TCR's.

Photoelectrochemical Etching and Dopant Selective Etch-Stops in SiC

One of the technological problems for SiC transducers is that the material is chemically inert, making micromachining difficult. There are a number of molten metals and molten salts [1] that attack SiC, but these are impractical for device fabrication due to the high temperatures involved. Device structures have been selectively etched in SiC using Reactive Ion Etching (RIE) [8]. However, the etch rates reported for RIE are too slow for many applications and RIE shows no selectivity between different conductivity types. Recently, we have developed a photoelectrochemical etching technique which has very high etch rates (up to 100 μm/min) and large selectivity between conductivity

types.

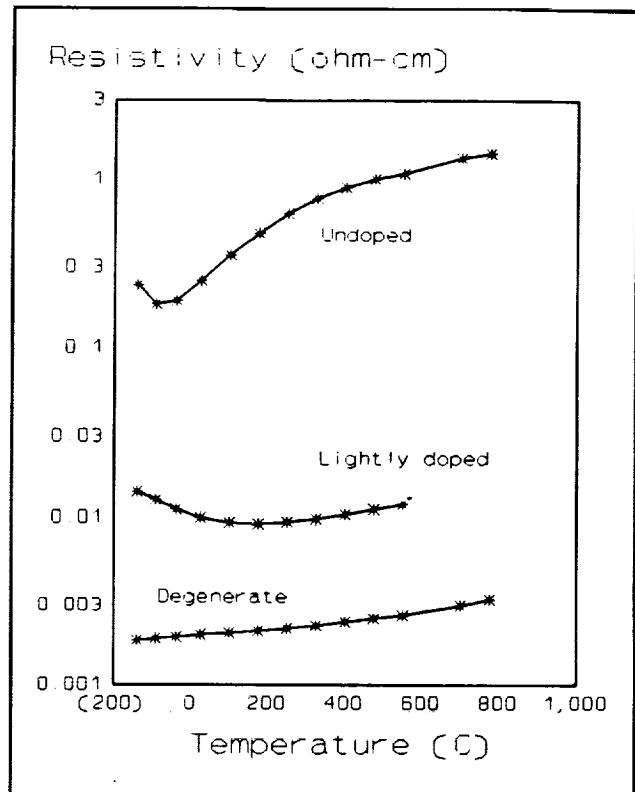The etch rates and process mechanism of SiC PEC etching have been described in an earlier publication [9]. Those results will be summarized here briefly for clarity. Fig. 5 is a diagram of the n-type ß-SiC/HF junction, which is similar in its charge transfer and energy band characteristics to a Schottky contact. At equilibrium, the Fermi level of the semiconductor lines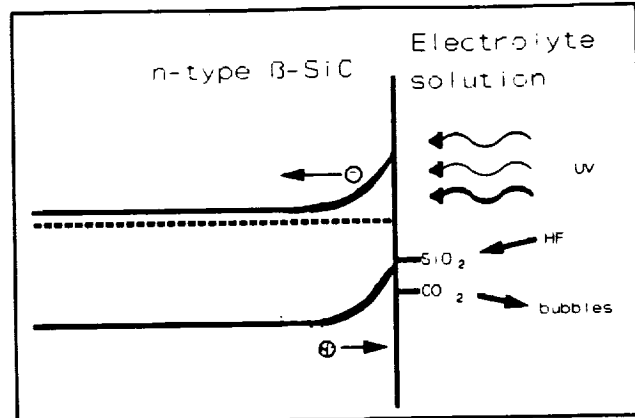 up with the redox potential of the solution, which for n-type material results in upward surface band-bending. Under these conditions, photocarrier generation near the surface will result in hole confinement at the surface, while electrons will be driven into the bulk. The holes that reach the surface are transferred into the solution, causing anodic oxidation of the SiC by H_2O. The reaction products, SiO_2 and CO_2 are removed from the surface by HF dissolution and bubbling, respectively.

Figure 5: Band diagram of the SiC/HF interface.

At certain potentials, p- and n-type SiC will exhibit the opposite band bending in HF solutions [10]. Thus, holes can be transported to the semiconductor/solution interface in the case of n-type material, while they will be confined in the bulk in p-type material. Therefore, a potential can be chosen where n-SiC will be etched and p-SiC will not, making dopant selective etch stops feasible.

High Temperature Ohmic Contacts for n-type ß-SiC Sensors

In order to fabricate high temperature sensors and other devices, it is necessary to develop ohmic contact metallizations that can withstand elevated temperatures. A variety of ohmic contact metallizations were investigated with contact resistivity measured as a function of anneal time in air. The metallizations were based on Ti and W ohmic contacts, which have contact resistivities as low as 10^{-4} Ω-cm^2. Several of the contact metallizations were stable after 10 hrs. at 650°C, while one system, based on a Ti ohmic contact, was able to withstand > 20 hrs. at 650°C with only a 30-40% increase in contact resistivity. Contact resistivity was measured using the four point probe method developed by Terry and Wilson [11] and modified by Kuphal [12].

References

1. Silicon Carbide-1973, ed. by R.C. Marshall, J.W. Faust and C.E. Ryan, (Univ. of S. Carolina Press, Columbia, South Carolina, 1974).
2. I.V. Rapatskaya, G.E. Rudashevskii, M.G. Kasaganova, M.I. Iglitskin, M.B. Reifman and E.F. Fedotova: *Sov. Phys. -Solid State* **9**, 2833 (1968).
3. G.N. Guk, N. Ya. Usol'tseva, V.S. Shadrin, and N.K. Prokop'eva: *Sov. Phys. Semicond.* **10**, 83 (1976).
4. J.A. Powell, L.G. Matus, and M.A. Kuczmarski: *J. Electrochem. Soc.* **134**, 1558 (1987).
5. C. Herring and E. Vogt: *Phys. Rev.* **101**(3) 944-961 (1956).
6. R. Kaplan, R.J. Wagner, H.J. Kim, and R.F. Davis: *Solid State Comm.* **55** (1) 67-69 (1985).
7. J.A. Freitas, S.G. Bishop, P.E.R. Nordquist Jr. and M.L. Gipe: *Appl. Phys. Lett.* **52**, 1695 (1988).
8. J.W. Palmour, R.F. Davis, P. Astell-Burt, and P. Blackborow in " Science and Technology of Microfabrication " ed. by R.E. Howard, E.L. Hu, S. Namba and S.W. Pang (Mat. Res. Soc., Pittsburg, 1987) p. 185.
9. J.S. Shor, X.G. Zhang and R.M. Osgood Jr.: J. Electrochem. Soc. **139**, 1213 (1992).
10. J.S. Shor, R.M. Osgood Jr. and A.D. Kurtz: Appl. Phys. Lett. **60**, 1001 (1992).
11. L.E. Terry and R.W. Wilson: Proc. IEEE **57**, 1580 (1969).
12. E. Kuphal: Solid State Electron. **24**, 69 (1981).

C-4